Integrative Biology

Dynamic Article Links

Cite this: *Integr. Biol.*, 2012, **4**, 945–952

www.rsc.org/ibiology

TECHNICAL INNOVATION

A high-throughput imaging system to quantitatively analyze the growth dynamics of plant seedlings†

Yongfan Men,‡[ab] Qiang Yu,‡[ac] Zitian Chen,[ad] Jianbin Wang,[bd] Yanyi Huang*[abd] and Hongwei Guo*[ac]

Received 3rd February 2012, Accepted 9th May 2012
DOI: 10.1039/c2ib20020a

Most current methods for analyzing the growth rate of plant seedlings are limited to low-throughput experimental configurations. We have developed an automatic system to investigate the dynamics of the growth of hypocotyls using *Arabidopsis* as model. This system is able to capture time-lapse infrared images of 24 seedlings automatically, with a spatial resolution of 2 μm per pixel and temporal interval of 5 min. Seedling length is rapidly calculated using automated geometric image-processing algorithms. With this high-throughput platform, we have investigated the genotype dependent difference of growth patterns, as well as the response to plant hormone – ethylene. Our analyses suggest that cytoskeleton function is not required in ethylene-induced hypocotyl inhibition. This novel integrative method can be applied to large-scale dynamic screening of plants, as well as any other image-based biological studies related to dynamic growth.

Introduction

Plant growth is accurately regulated by gene expression and has characteristic spatio-temporal patterns.[1–3] The spatial distribution of gene expression is reflected in different phenotypes at different positions, such as root tip and hypocotyl hook.[4] Meanwhile, the temporal gene expression profile is highly associated with growth rates of different parts of the plant at specific time points.[5] Many conventional technologies have been applied to measure spatial and temporal gene expression, including microscopy,[3] fluorescence detection,[6] and electrophoresis.[7] However, most of them are based on end-point analysis, leading to conclusions without dynamic information.

The hypocotyl is the stem of germinating seedling and is a particularly important organ. When the seedling is beneath the soil, the hypocotyl elongates rapidly due to the absence of visible light. The growth of hypocotyl is highly sensitive to environmental factors, including light and external hormones, making it a perfect model system to study the regulation networks and pathways in plants.[8–11] A method that can reveal the details of the growth process, especially the precise changes in growth rate, has been long-awaited. It is also difficult for conventional methods to investigate into the rapid responses to external stimuli (*e.g.* plant hormones)[12] and gene regulations. Dynamic analysis[13] has become a powerful tool to resolve the details of growth rate,[14] as well as oscillatory growth patterns.[15,16]

[a] *Biodynamic Optical Imaging Center, College of Life Sciences, Peking University, Beijing 100871, China. E-mail: yanyi@pku.edu.cn, hongweig@pku.edu.cn*
[b] *College of Engineering, Peking University, Beijing 100871, China*
[c] *State Key Laboratory of Protein and Plant Gene Research, College of Life Sciences, Peking University, Beijing 100871, China*
[d] *College of Chemistry and Molecular Engineering, Peking University, Beijing 100871, China*

† Electronic supplementary information (ESI) available. See DOI: 10.1039/c2ib20020a.

‡ These authors made the equal contribution to this work.

Insight, innovation, integration

We developed an automatic and high-throughput infrared imaging system that greatly improves the quantitative analysis of growth dynamics of plant seedlings. It is a technical innovation that combines instrumentation and algorithm development for accurately assessing the growth rate of hypocotyls. We employ this system to quantitatively study *Arabidopsis* seedling growth dynamics, which is critical to understand the gene regulation of plants, to quantify the responses to gaseous hormones, and to screen mutants for functional phenotypes. The integration between the automatic microscopic time-lapse imaging system and the universally applicable image-processing algorithm greatly facilitates our study of multiple samples in parallel. This system also substantially eliminates the need for human power and reduces the error in measurement.

Arabidopsis is a popular model plant[17,18] because it self-pollinates, has short growth-period, and a small genome size. Additionally, the whole genome of *Arabidopsis*[19] has been sequenced, making it ideal for study of gene regulatory effects. Meanwhile, thanks to the small physical size of the *Arabidopsis* seedling, they are ideal for dynamic behaviour study and high-throughput experiments.

The key step of dynamic observation and analysis is accurate measurement, through which physical properties of samples can be converted to quantitative values at certain time points. The growth dynamics of *Arabidopsis* hypocotyls, which are typically only a few millimeters to a few centimeters in length, must be monitored using high precision techniques. Many approaches have been taken to study the growth of *Arabidopsis*. For instance, growth rate of the root has been measured by physically adjusting water surface, which touched the tip of the growing root.[20] In another approach to measure hypocotyl growth rate, a transducer is connected to the apical hook with a hair.[21] CCD cameras have also been used to image and measure the length of growing seedlings at certain time intervals.[22] This image-based approach has been applied to analyze *Arabidopsis*' growth responses to ethylene,[23] light,[24] as well as shade influence.[25]

Herein we report a novel approach to perform high-throughput studies of the growth dynamics of *Arabidopsis* seedlings. With this imaging-based system, we can monitor 24 samples in a single experimental run. Both image acquisition and image analysis steps are automatically executed to achieve objective results with minimum human interference. We have built an infrared illumination system to capture high-quality images with resolution better than 2 μm pixel^{-1}. We have also developed two new algorithms to robustly track the stems of seedlings, and to determine their length. Over 60% of the seedlings can be well processed and accurately calculated through the algorithms, and produce precise data for growth assessment. The major advantage of this algorithm is the accurate assessments of the central line and terminus in each image. This method has great potential to be applied to study many organs of plant seedlings, such as the hypocotyl and root.

Experimental methods

Infrared imaging system

A schematic diagram of the setup is shown in Fig. 1a. An 11-Mega pixel (4008 × 2672) monochrome CCD camera (QHY11, Star Sense Technology, Beijing, China) was used for image capturing. The dimension of the CCD sensor is 36 × 24 mm and the physical size of each pixel is 9.0 × 9.0 μm. We used a photographic macro lens (MP-E 65 mm f/2.8, Canon, Japan) to match this sensor for obtaining magnified (∼5×) images of the *Arabidopsis* seedlings with resolution better than 2 μm/pixel. A manual translational stage was used to hold the lens with camera and to adjust the focus.

Arabidopsis seedlings were placed on top of agar plates, which were formed by curing agar in square petri dishes. We used three plexiglass chambers (100 × 150 × 200 mm) to control the microenvironments of the samples. Each chamber had a gas inlet on the top and an outlet on the bottom of the chamber. During experiment, we kept the airflow at 100 ml min^{-1}. We used manual reducing valves to adjust the concentration of the ethylene in the input gas mixture, with a stable concentration of 20 ppm (part per million) of ethylene gas during treatments. The position of each chamber could be accurately adjusted by three manual stages (Fig. S1, ESI†). Three motorized translational stages (KSA400-12-X and KSA200-11-X, Zolix Instrument, Beijing, China) were used to switch between the samples for imaging. A fourth motorized vertical stage (PSA30-ZF, Zolix Instrument, Beijing, China) was used to adjust the z position of the camera. The motion of the stages was controlled by a computer through a multi-channel stepper motor controller (MC600, Zolix Instrument, Beijing, China). We have confirmed that the reposition precision of the stages is less than 2 μm, which would result in about 1-pixel difference in the CCD sensor for image capture. In a typical experiment we captured the images every 5 min, and the seedlings would grow 50–300 μm (25–150 pixels in the images), which can be easily resolved using our system.

To investigate the growth rate of the seedlings *via* image acquisition without stimuli of visible light,[26,27] we used 940 nm infrared light sources to illuminate the sample for image acquisition. Two sets of IR LEDs were used in our system. One was a square array of IR LEDs sitting at the back of the sample for focus adjustment. The other consisted of 3 IR LED arrays to illuminate the samples from both sides and the top at back (Fig. 1a). To avoid heat effect of light sources, samples were illuminated only during image acquisition through computer control. We found that to reduce water condensation along the stems of the seedlings, which otherwise interferes with image processing, it was better to use side illumination, instead of back illumination.

The whole setup was constructed on an optical table, and covered by opaque cloth throughout the experiment to avoid visible light illumination. All experiments were carried out in a phytotron at 22 °C.

Seedling preparation

The substrate was prepared by pouring Murashige and Skoog basal salt mixture (4.33 g L^{-1} Murashige and Skoog salt,[28] 10 g L^{-1} cane sugar, 15 g L^{-1} agar, pH 5.7–5.8, autoclaved with high pressure) into square dishes. *Arabidopsis* seeds were soaked with 75% ethanol with 0.05% Triton X-100 for 10 min to sterilize the surface. We manually picked the plump seeds with tweezers, sowed them onto substrate, and aligned them in lines at intervals ∼7.5 mm. We usually placed 13 seeds per line and 2 lines in each dish.

We kept the sample dishes in darkness at 4 °C for 4 days, and then raised the temperature to 22 °C under visible light for 12 h to induce germination. We then wrapped the sample dishes with aluminium foils and placed them vertically into an incubator at 22 °C for another 22 h. Then we transferred the sample dishes into the phytotron, unwrapped the foil and mounted the dishes into chambers. A small cup of water was also placed in each chamber to maintain the humidity.

Alignment and automation

The depth of focus of our imaging system was typically smaller than 500 μm. To guarantee that all images were in focus while

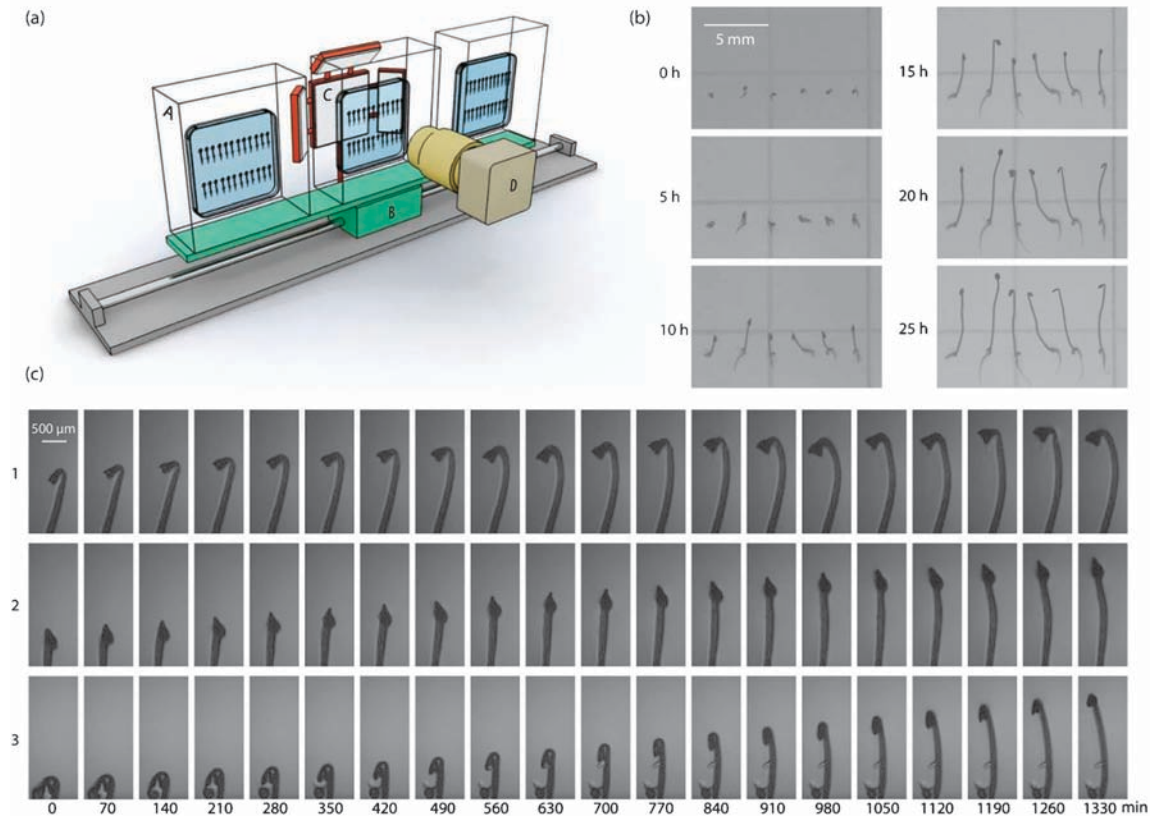

Fig. 1 (a) The schematic construction of the imaging system. A: PMMA chamber, B: long-range linear translational stage, C: IR light sources on a short-range translational stage, D: CCD camera with macro lens on a short-range translational stage and a vertical stage. (b) The pictures of 6 wild-type seedlings during growth. (c) Time-lapse images clearly show the non-identical appearances of three seedlings with identical genotype Col-0 during the growth.

samples were moved back and forth, we had to carefully adjust the position of each sample dish before the experiment. All sample dishes should be mounted perpendicularly to the optical axis of the imaging system. The sample position was adjusted using linear and rotational stages that held the sample chambers (Fig. S1†). Once both the first and the last seedlings in a line were adjusted within focus, the whole line of seedlings was also in focus because of the perfect flatness of the agar substrate.

We used a home-developed Matlab script to control the whole system automatically. The ethylene introduction and air purge were controlled through solenoid valves. Motorized translational stages were coupled with the imaging system for fully automatic operation (Fig. 1a). A long-range translational stage was constructed to hold and manipulate three chambers which each contain a single agar plate (seedling array). We use two short-range translational stages (not shown in the Fig. 1a) to move the light sources and the camera, respectively. The long-range translational stage brings the chambers one at a time in between the light sources and the camera for imaging and the synchronized short-range stages move the camera and light sources in order to image individual seedlings within the chamber. We use short-range translational stages to move the camera and light sources instead of moving the chambers when scanning seedling arrays in order to avoid vibration of the chamber. With this approach, we achieve an imaging rate as high as 12 images min^{-1}. In the event that the seedlings grow beyond the field of view of the camera, the vertical position of the camera was adjusted, making sure the whole cotyledon was always fully captured. This may happen a few times per experiment at regular intervals.

Results and discussion

Previously reported dynamic analysis methods, which determine growth rate through time-lapse images, have demonstrated accurate measurement of tiny changes during seedling growth. However, these methods, whose image processing is usually tedious and time-consuming, still face many challenges.

Most of these approaches require extensive human interference, including sample adjustment and length measurement, and thus have many limitations. Previous approaches can only observe and measure one or two seedlings in a single experimental run, limiting the throughput. To perform statistical analysis, either multiple setups or multiple repeats are required. This is not only resource consuming, but also difficult to maintain consistent experimental conditions, reducing reproducibility of the experiments. For long-term observation, automatic position adjustment is desired so that seedlings would not grow out of the field of view, which is merely a fraction of a centimetre. Automated systems also have the potential to reduce human error and improve accuracy. As we will show, the automated system described in this paper achieves long-term, high-throughput observation of seedling growth with minimum human intervention. Another major disadvantage of

previously reported methods is that they are limited to studies of specific morphological phenotypes. The terminus determination, which is critical for seedling length calculation, is done either by targeting the highest grey value area within the gap produced by the bifurcation of the two petioles at the cotyledonary node,[29] or by calculating the maximum Euclidean distance transform value in the bulge area that forms by shoot apical where the petioles initiate.[25] Both approaches require the cotyledonary node to be visible in the image. This requirement becomes impractical because most seedlings are not perfectly oriented for ideal morphological projections. Actual samples have a variety of appearances (for example, see Fig. 1b). Most are difficult to be analysed by existing image processing algorithms, simply because their appearances are not suitable. Moreover, it is not rare for seedlings to change morphology (Fig. 1c). Although manual measurement and larger scale sampling may partially solve the problem, a universal image processing method is highly desired.

Here we introduce our own image processing method, which calculates growth rate through time-lapse images acquired under IR illumination. We started our process by suppressing the background and reducing the noise of the raw images, using top-hat transform. This process also helped to sharpen the edges of seedlings, and enhance the contrast. After the background was removed, we converted the gray scale images into binary ones for further analysis. In this step it was important to determine the suitable threshold. During the growth, the shape and transmission of the seedlings changed gradually and constantly and the threshold was automatically adjusted accordingly. Noises were further suppressed and edges smoothed.

To make accurate measurements, we developed a novel method to determine the central line of the seedling (Fig. 2). When a seedling changed its location, we firstly confirmed the position of the central line, which represented the centre of the seedling. Two approaches were developed and evaluated. The first approach is shown as Fig. 2a. Starting from the bottom of the picture, we first determine the central point A in the middle of the seedling along the bottom line, and then use this point to estimate the next central point B with a small interval AB along the vertical line. Since each seedling grows in a different direction, this estimation may not be accurate and needed adjustment. To get the actual central point C, we calculated the length and orientation of BE and BG and used the equation $BC = |(BE - BG)|/(1 + \cos\angle EBG)$. By repeating this operation, the central line of the seedling can be found. This approach, although highly accurate, is time-consuming due to the multi-step calculation for each point.

The second approach starts from producing an estimated line that runs through the seedling from bottom to top. A series of points along the line with small intervals in-between are abstracted and amended to actual central points, as shown in Fig. 2b. We used either watershed or skeleton functions to create a central line of the seedling, and then amended the points. This approach is more efficient and slightly more stable than the first one. However, because intervals between points are fixed, for seedlings with large curvatures, it is often difficult to process. To solve the problem, we combined the above two approaches by extracting and amending a central line first and then made fine adjustments along large curvatures by adding more points.

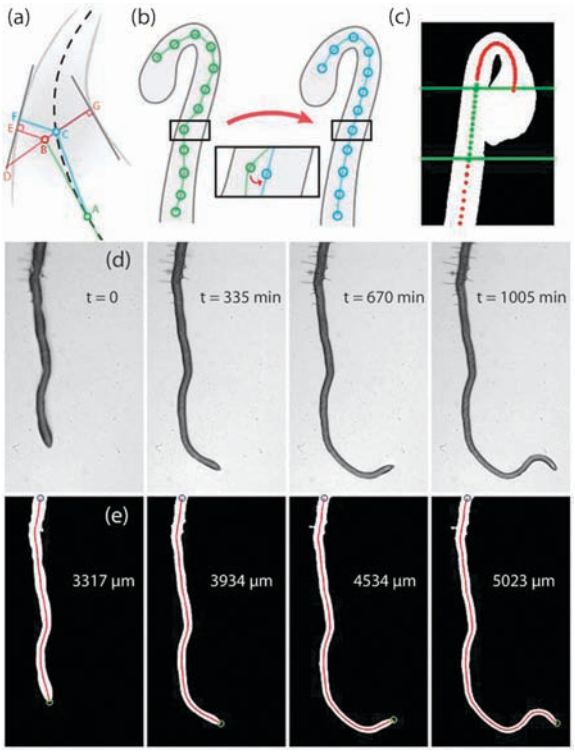

Fig. 2 The algorithms of image processing and central line determination. (a) The core algorithm of correcting a central point. A is the previous central point; B is the estimation of the next central point based on A; C is the corrected central point, through which CF = CG. (b) The method of correcting the central line of a seedling. We create a rough skeleton (line in green) of a seedling through image processing and picked the points with a given displacement in between. We then fine-adjusted each point to obtain an amended central line (blue). (c) A demonstration of accurate determination of the central line of a seedling with the complex shape of apex. (d) The images of a root growing with IR illumination. (e) The calculation results of above images. The red lines are calculated central lines; the blue and green circles represent start points and terminus (root tips) of each image.

For those images of seedlings in which the cotyledon touches the hypocotyl, the determination of the central line becomes challenging. We divided the seedling apex into three parts and applied a multi-stage calculation to track the seedling's skeleton, as shown in Fig. 2c and Supplementary Movie 1, ESI†. In the lower and upper parts, we used the first approach mentioned above to determine the central points (red dots). For the section between two green lines, we amended originally assigned central points to corrected ones (green dots). The distance between two adjacent central points is dynamically adjusted with the curvature of the feature, ensuring the accuracy of the length calculation. The method can also be applied to measure root growth dynamics, even when the shape of the root is irregular (Fig. 2d and e and Supplementary Movie 2†).

To calculate the length of the seedlings by measuring the central lines, we have to overcome another challenge: how to determine the terminus. During our experiments, growth mostly happens in the hypocotyls. Manual and computer-aided measurements have all been tried before, but they are either imprecise or limited to certain shapes of cotyledon. Our approach (Fig. 3)

introduces a novel algorithm by comparing adjacent images. We cropped the apex part (the cotyledon) of the first image and then did an exclusive disjunction (also called "exclusive or", or XOR) logical operation between this cropped region and the second image in the time-lapse series. The whole process of this operation has been illustrated in Fig. 3. A square image patch with the center at position (x_0,y_0) containing the seedling apex is cropped from the image i. Then, the image patch is placed on the image $i + 1$, with the center at position (x,y). For each (x,y), we calculated the similarity between the patch and the image $i + 1$ through XOR operation. XOR operation can generate a digital output from two digital inputs. Two different inputs generate "1", while same inputs generate "0". At every (x,y) position, we calculated the similarity by summing up the XOR output of each pixel. The lowest value of the sum indicated the most-matched location, which is the terminus point (x_1,y_1) in image $i + 1$. At this terminus point (x_1,y_1), we crop a new patch from image $i + 1$, and place it on the image $i + 2$. Through the same procedure, we can get the (x_2,y_2). Repeating this procedure will calculate the terminus in all images. This method allows us to quickly locate the most similar point between two images, as demonstrated in Fig. 3a and b.

We applied this method to the serial images of growing hypocotyl, as shown in Fig. 3c. The result of the XOR operation can be illustrated as a colour-map and the highest similarity can be clearly observed in the map (peaks in Fig. 3c), indicating the location of the terminus in the whole series of images. Although in each series the terminus of the first image can be determined automatically, we do this manually to be more precise. The calculation of the subsequent images was performed automatically. Thus with the couple of minutes needed for the manual determination of the apex location of 24 first images, hours to days of data can be automatically processed with greater precision.

In general, determination of the absolute position of the terminus (the central point of the box in Fig. 3c and d) is not

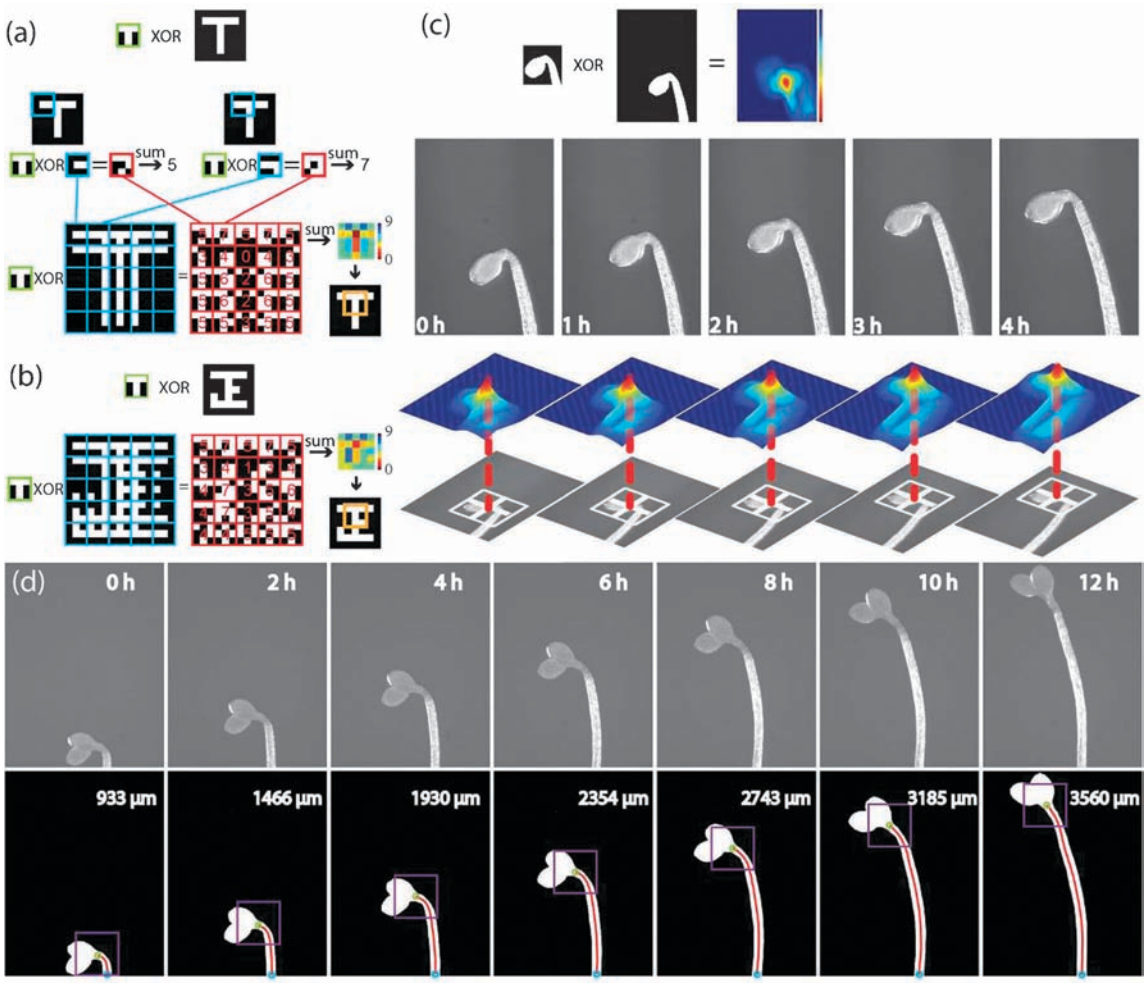

Fig. 3 The determination of the terminus in each image using exclusive disjunction (XOR) operation. (a) Demonstration of the XOR operation between a small patch (green) and a simple image. When the patch is placed onto the image (indicated as a blue patch), the sum of XOR operation between corresponding pixels will represent the similarity between patches. Lower the score is, higher the similarity will be. By scanning through the whole image with XOR operation, the position with highest similarity is located (brown). (b) XOR operation is applicable to more complicated images. (c) Terminus determination of seedlings with XOR operation. The operational result is shown as a color-map and the peak shows higher similarity. (d) The terminus-tracking algorithm accepts evolving changes in the images. We demonstrate a real example of terminus tracking of a seedling that during its hypocotyl elongation, the cotyledon changes the orientation.

critical to the tracking process since the growth rate was defined as the hypocotyl length difference between images. However the terminus within the same series of images should be consistent. Since we acquire images of each seedling every 5 min, the shapes of the apex did not change very much in two adjacent images. Our algorithm shows great tolerance to the shapes of the apex, allowing us to accurately track the terminus through evolving apex shapes, as shown in Fig. 3e and Supplementary Movie 3†.

Once coordinates of all central points and terminus are decided, we can calculate the length of all seedlings at each time-point and plot their growth curves. The growth rate curves, shown as Fig. 4, are obtained by differentiating the growth curves. We measured the long-term (60 h) growth patterns of three common genotypes of *Arabidopsis* seedlings: the wild type Col-0, and two mutant seedlings *ein2*, and *ein3 eil1*. The last two show hypocotyl insensitivity to ethylene application. The spatial resolution of our system is 2 μm/pixel and the temporal interval between images of each seedling is 5 min, allowing us to pick up small variations in growth rate. This short interval is critical since the ethylene reaction may drastically slow down the growth rate, from 300 μm h^{-1} to 100 μm h^{-1} in about 10 min.

Our method provides a high-throughput way to monitor multiple seedlings in a single run. From the smoothed curves, we find that the growth rates vary between 100 and 500 μm h^{-1} and the change can be rapid. The measurement starts 48 h after the 12 h-long visible light illumination period, which triggers germination. Growth pattern differences among genotypes are apparent, as shown in Fig. 4. Generally speaking, the growth rate of Col-0 is more stable than the mutant seedlings. Both mutants show a peak of growth rate during this period, and the *ein2* mutant can reach a maximum growth rate of 560 μm h^{-1}, almost twice of the maximum growth rate of Col-0. This genotype-dependent growth pattern suggests that caution must been taken in interpreting growth behaviours induced by environmental stimulations. Determining the proper time windows for measurement is critical. It has been suggested[14,23,25] that dynamic analysis of seedling growth needs to be performed in specific time windows, which represent stable growth phases. Our observation shows that these three genotypes all reach a relatively stable growth period after 80 h and exhibit a comparable growth rate of 150–200 μm h^{-1}.

Ethylene has been documented to be one of the most powerful plant hormones to hinder the growth of hypocotyl and root.[20,30] We perform the ethylene treatment to examine the dynamic responses of these 3 genotypes, as shown in Fig. 5a. Col-0 is sensitive to ethylene treatment (20 ppm) and the growth rate drops to less than 40% of the original value within 1 h. The growth rate of *ein3 eil1* slightly drops (change $<10\%$) about 10 min after the ethylene is added and is recovered about 100 min later, while *ein2* did not show any change in the growth rate.

It has been reported that there is a two-phase reduction of growth rate for Col-0 under the ethylene treatment.[23] First there is a rapid reduction phase followed by a slow reduction phase. This is confirmed by Col-0's curve in Fig. 4a. The response of Col-0 to the withdrawal of ethylene is also prompt (Fig. 5b). The whole experiment is carried out in a single run and data processing is automatic.

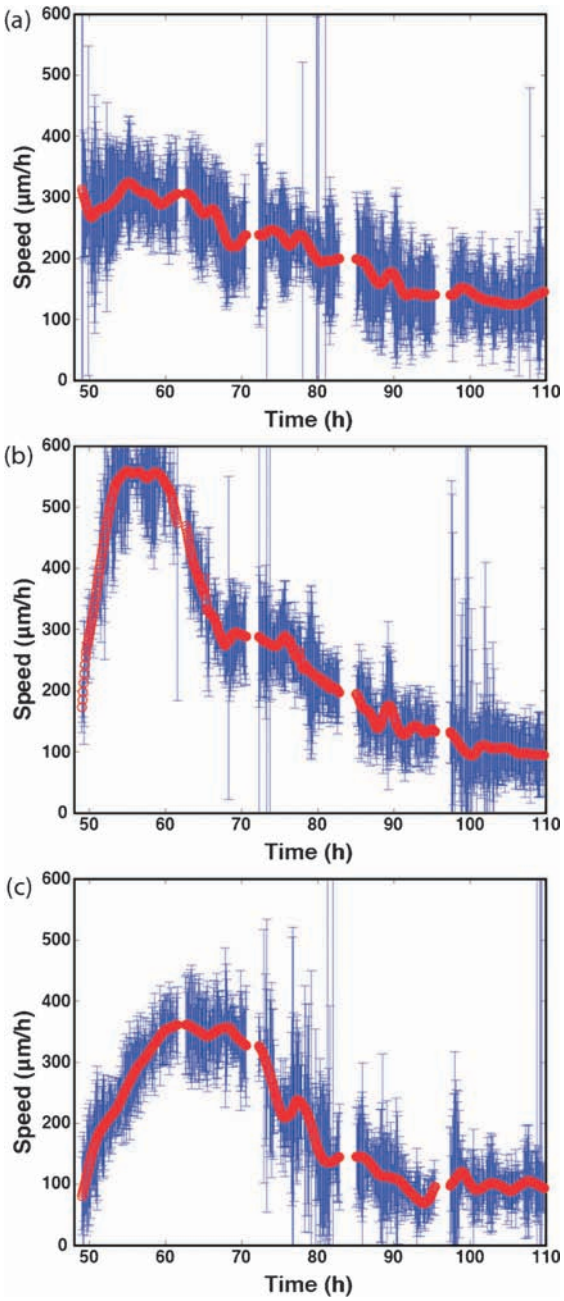

Fig. 4 The hypocotyl growth rate of the three genotypes in air. (a) Wild type Col-0. (b) The *ein2* mutant. (c) The *ein3 eil1* mutant. Data present Mean ± 50 μm h^{-1}, $n = 8$. Red circles indicate statistic average. The time axis represents the growth time of in the dark after visible light illumination. Each curve has a few breaks, which are due to the vertical position adjustment and re-focusing of the camera for long-term observation.

The increased accuracy and throughput of our system allow us to perform dynamic screening of drugs using growth rate as read-out. Four chemicals, phalloidin, oryzalin, taxol, and latrunculin A, have been reported to interfere with the function of cytoskeleton,[31–33] and should consequently affect the growth rate of seedlings. We have investigated the effect of these four chemicals on ethylene-induced growth inhibition. The experiments, including 4 treatments of drugs and the control group,

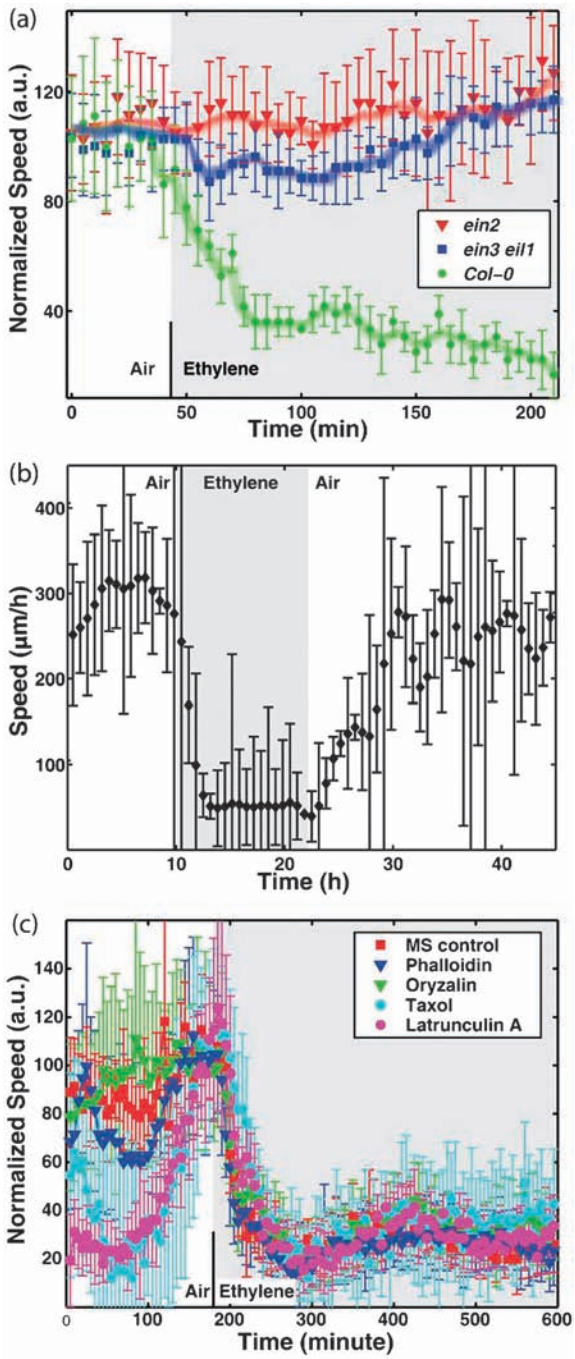

Fig. 5 The ethylene response curves (a) Normalized growth rates of wild type Col-0, the *ein2* and *ein3 eil1* mutant upon treatment of 20 ppm ethylene gas. For each genotype, the normalized data were calculated relative to the value at time 0. (b) Growth rate of wild type Col-0 with initially ethylene introduction and subsequently ethylene removal. (c) Normalized growth rates of wild type Col-0 grown on the medium supplemented with different drugs. For each drug treatment, the normalized data were calculated relative to the value at the time point when ethylene was introduced.

were carried out through 5 individual runs. Each run contained 24 seedlings in 3 chambers. As expected, the growth rates of Col-0 seedlings upon treatment of the four chemicals are reduced by 23%–60%, compared with the untreated controls at 300 μm h^{-1} (data not shown). Nevertheless, we find that the treatment with each chemical has little effect on the seedling response to ethylene (Fig. 5c). For all seedlings, the growth rate drops to 20% of the original value before adding ethylene. This result suggests that the inhibitory effect of ethylene on hypocotyl growth might be irrelevant to cytoskeleton function.

Conclusions

In summary, we have designed and constructed an automatic system to perform dynamic observation and analysis of seedling growth. This system is able to carry out three experiments simultaneously with 8 seedlings in each. With this high-throughput configuration, measurement of high accuracy and great reproducibility unveils the growth rate of each sample at given time points and the dynamics of growth rate. Our demonstrations on the growth pattern observation of different genotypes of *Arabidopsis*, their dynamic responses to ethylene introduction and removal, as well as the finding of the lack of cytoskeleton function in ethylene-induced growth inhibition, clearly show the potential of this novel approach in plant biology research. Beside hypocotyls, this method can be applied to roots as well. With further integration and improvement of the speed of image acquisition and processing, we envisage this system can be applied to larger scale screening of mutants with subtle or transient growth phenotypes.

Acknowledgements

The authors thank Dr Hongyun Qiu and Ying Zhou for their advice on instrumentation and image processing, and Dr Aaron Streets for the advice on manuscript revision. This work was supported by the National Natural Science Foundation of China (Grant No. 90913011), the Ministry of Science and Technology of China (Grant No. 2011CB809106), the Fok Ying Tung Educational Foundation, and the Instrument and Technology Development Project of Peking University.

Notes and references

1 A. M. Koltunow, J. Truettner, K. H. Cox, M. Wallroth and R. B. Goldberg, *Plant Cell*, 1990, **2**, 1201–1224.
2 J. B. Bahme and M. N. Schroth, *Phytopathology*, 1987, **77**, 1093–1100.
3 A. V. Broek, J. Michiels, A. Vangool and J. Vanderleyden, *Mol. Plant-Microbe Interact.*, 1993, **6**, 592–600.
4 K. Birnbaum, D. E. Shasha, J. Y. Wang, J. W. Jung, G. M. Lambert, D. W. Galbraith and P. N. Benfey, *Science*, 2003, **302**, 1956–1960.
5 L. Pnueli, M. Abuabeid, D. Zamir, W. Nacken, Z. Schwarzsommer and E. Lifschitz, *Plant J.*, 1991, **1**, 255–266.
6 T. Egener, T. Hurek and B. Reinhold-Hurek, *Mol. Plant-Microbe Interact.*, 1998, **11**, 71–75.
7 R. MedinaSuarez, K. Manning, J. Fletcher, J. Aked, C. R. Bird and G. B. Seymour, *Plant Physiol.*, 1997, **115**, 453–461.
8 A. vonArnim and X. W. Deng, *Annu. Rev. Plant Physiol. Plant Mol. Biol.*, 1996, **47**, 215–243.
9 E. Gendreau, J. Traas, T. Desnos, O. Grandjean, M. Caboche and H. Hofte, *Plant Physiol.*, 1997, **114**, 295–305.
10 P. Zadnikova, J. Petrasek, P. Marhavy, V. Raz, F. Vandenbussche, Z. J. Ding, K. Schwarzerova, M. T. Morita, M. Tasaka, J. Hejatko, D. Van Der Straeten, J. Friml and E. Benkova, *Development*, 2010, **137**, 607–617.

11 F. Vandenbussche, J. Petrasek, P. Zadnikova, K. Hoyerova, B. Pesek, V. Raz, R. Swarup, M. Bennett, E. Zazimalova, E. Benkova and D. Van Der Straeten, *Development*, 2010, **137**, 597–606.
12 M. L. Evans, *Annu. Rev. Plant Physiol.*, 1974, **25**, 195–223.
13 D. J. Cosgrove, *Plant Physiol.*, 1981, **68**, 1439–1446.
14 B. M. Binder, *J. Plant Growth Regul.*, 2007, **26**, 131–142.
15 G. B. Monshausen, T. N. Bibikova, M. A. Messerli, C. Shi and S. Gilroy, *Proc. Natl. Acad. Sci. U. S. A.*, 2007, **104**, 20996–21001.
16 L. C. Roden and R. A. Ingle, *Plant Cell*, 2009, **21**, 2546–2552.
17 R. E. Pruitt and E. M. Meyerowitz, *J. Mol. Biol.*, 1986, **187**, 169–183.
18 V. Walbot, *Nature*, 2000, **408**, 794–795.
19 S. Kaul, H. L. Koo, J. Jenkins, M. Rizzo, T. Rooney, L. J. Tallon, T. Feldblyum, W. Nierman, M. I. Benito, X. Y. Lin, C. D. Town, J. C. Venter, C. M. Fraser, S. Tabata, Y. Nakamura, T. Kaneko, S. Sato, E. Asamizu, T. Kato, H. Kotani, S. Sasamoto, J. R. Ecker, A. Theologis, N. A. Federspiel, C. J. Palm, B. I. Osborne, P. Shinn, A. B. Conway, V. S. Vysotskaia, K. Dewar, L. Conn, C. A. Lenz, C. J. Kim, N. F. Hansen, S. X. Liu, E. Buehler, H. Altafi, H. Sakano, P. Dunn, B. Lam, P. K. Pham, Q. Chao, M. Nguyen, G. X. Yu, H. M. Chen, A. Southwick, J. M. Lee, M. Miranda, M. J. Toriumi, R. W. Davis, R. Wambutt, G. Murphy, A. Dusterhoft, W. Stiekema, T. Pohl, K. D. Entian, N. Terryn, G. Volckaert, M. Salanoubat, N. Choisne, M. Rieger, W. Ansorge, M. Unseld, B. Fartmann, G. Valle, F. Artiguenave, J. Weissenbach, F. Quetier, R. K. Wilson, M. de la Bastide, M. Sekhon, E. Huang, L. Spiegel, L. Gnoj, K. Pepin, J. Murray, D. Johnson, K. Habermann, N. Dedhia, L. Parnell, R. Preston, L. Hillier, E. Chen, M. Marra, R. Martienssen, W. R. McCombie, K. Mayer, O. White, M. Bevan, K. Lemcke, T. H. Creasy, C. Bielke, B. Haas, D. Haase, R. Maiti, S. Rudd, J. Peterson, H. Schoof, D. Frishman, B. Morgenstern, P. Zaccaria, M. Ermolaeva, M. Pertea, J. Quackenbush, N. Volfovsky, D. Y. Wu, T. M. Lowe, S. L. Salzberg, H. W. Mewes, S. Rounsley, D. Bush, S. Subramaniam, I. Levin, S. Norris, R. Schmidt, A. Acarkan, I. Bancroft, F. Quetier, A. Brennicke, J. A. Eisen, T. Bureau, B. A. Legault, Q. H. Le, N. Agrawal, Z. Yu, R. Martienssen, G. P. Copenhaver, S. Luo, C. S. Pikaard, D. Preuss, I. T. Paulsen, M. Sussman, A. B. Britt, D. A. Selinger, R. Pandey, D. W. Mount, V. L. Chandler, R. A. Jorgensen, C. Pikaard, G. Juergens, E. M. Meyerowitz, A. Theologis, J. Dangl, J. D. G. Jones, M. Chen, J. Chory, M. C. Somerville and A. G. In, *Nature*, 2000, **408**, 796–815.
20 W. E. Rauser and R. F. Horton, *Plant Physiol.*, 1975, **55**, 443–447.
21 B. M. Parks, M. H. Cho and E. P. Spalding, *Plant Physiol.*, 1998, **118**, 609–615.
22 B. M. Parks and E. P. Spalding, *Proc. Natl. Acad. Sci. U. S. A.*, 1999, **96**, 14142–14146.
23 B. M. Binder, R. C. O'Malley, W. Y. Wang, J. M. Moore, B. M. Parks, E. P. Spalding and A. B. Bleecker, *Plant Physiol.*, 2004, **136**, 2913–2920.
24 N. D. Miller, B. M. Parks and E. P. Spalding, *Plant J.*, 2007, **52**, 374–381.
25 B. Cole, S. A. Kay and J. Chory, *Plant J.*, 2011, **65**, 991–1000.
26 K. M. Folta and E. P. Spalding, *Plant J.*, 2001, **26**, 471–478.
27 K. M. Folta, M. A. Pontin, G. Karlin-Neumann, R. Bottini and E. P. Spalding, *Plant J.*, 2003, **36**, 203–214.
28 T. Murashige and F. Skoog, *Physiol. Plant.*, 1962, **15**, 473–497.
29 L. Y. Wang, I. V. Uilecan, A. H. Assadi, C. A. Kozmik and E. P. Spalding, *Plant Physiol.*, 2009, **149**, 1632–1637.
30 A. B. Bleecker, M. A. Estelle, C. Somerville and H. Kende, *Science*, 1988, **241**, 1086–1089.
31 M. A. Jordan and K. Kamath, *Curr. Cancer Drug Targets*, 2007, **7**, 730–742.
32 E. A. Perez, *Mol. Cancer Ther.*, 2009, **8**, 2086–2095.
33 P. G. Morris and M. N. Fornier, *Clin. Cancer Res.*, 2008, **14**, 7167–7172.

Electronic Supplementary Material (ESI) for Integrative Biology

Supporting Information

A high-throughput imaging system to quantitatively analyze the growth dynamics of plant seedlings

Yongfan Men[¶1,2], Qiang Yu[¶1,3], Zitian Chen[1,4], Jianbin Wang,[2,4] Yanyi Huang*[1,2,4], and Hongwei Guo*[1,3]

[1] Biodynamic Optical Imaging Center, College of Life Sciences, [2] College of Engineering, [3] State Key Laboratory of Protein and Plant Gene Research, College of Life Sciences, and [4] College of Chemistry and Molecular Engineering, Peking University, Beijing 100871, China

[¶] These authors made the equal contribution to this work.

*Correspondence should be addressed to H. G. (hongweig@pku.edu.cn) or Y. H. (yanyi@pku.edu.cn).

1. Supporting Figure

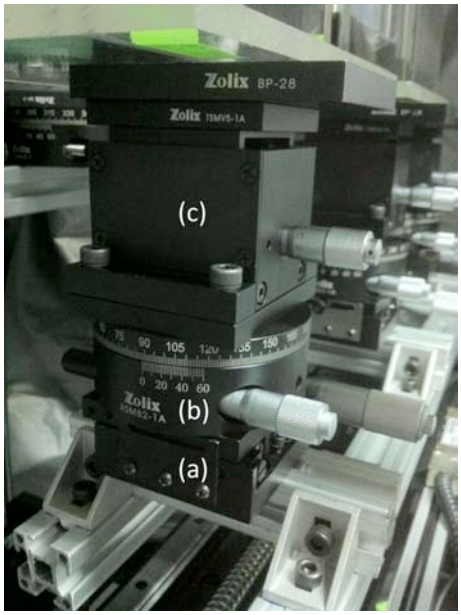

Fig. S1 Three horizontal (TSM25-1A, Zolix Instrument, Beijing, China), rotational (RSM82-1A, Zolix Instrument, Beijing, China), and vertical (TSMV5-1A, Zolix Instrument, Beijing, China) stages that hold the sample chambers are shown in the figure as (a), (b), and (c), respectively. The stages are constructed vertically, and fixed on the automated translational stage by aluminum frame.

2. Supporting Movies

Movie S1. The calculation process illustrated by the first approach described in the paper. In the movie, the algorithm is able to proceed even when the cotyledon is touching the hypocotyl. The seedling is divided into geometrically different regions. In each region, different rules are applied to determine the middle points. The whole middle line determination is divided into 4 stages. In the first

stage, the middle points in the hypocotyl below the red line are determined with a large step size. The yellow line shows the calculation direction. The grey circle highlights the middle point centering but is not used in the calculation. In the second stage, the step size is decreased. This operation ensures the calculation can run smoothly into the third stage. In the third stage, the step size is further decreased, to accommodate the high curvature of the hook. In the last stage, the points in the second stage are amended, and the middle line calculation is finished.

Movie S2. The tracking of the seedling terminus when cotyledon is growing and changing its orientation. The red box is the patch that is used to track the endpoint. The blue and green circles show the starting and ending point of the middle line, respectively. The red line shows the whole middle line. The length of the middle line is shown in each frame.

Movie 3. The calculation of the root of the seedling. The blue and green circles show the starting and ending point of the middle line, respectively. The red line shows the whole middle line. The length of the middle line is shown in each frame. The terminus of the middle line is determined from the intersection between the middle line and the edge of the root tip.

3. Supporting Algorithms.

Note: The source code is highly integrated with the hardware system, thus cannot be simply proceeded on other machines without further modifications. Here we present our key algorithms using pseudo code with explanations below. The readers are welcome to contact with the authors for comments or questions in detail.

```
Certain scripts, including the image processing procedures, are omitted
as they are neither essential for applying the idea nor mentioned in the
paper.

% Part 1:
% Pseudocode: central-line calculation.
% --------
% basic data structure is a "point" ('p' in scripts below):
% point.c=[x,y] - the x,y coordinate of the point
% point.v - the tangent direction of the point
% point.rl and point.rr - left and right radius length of the point
% point.vl and point.vr - left and right radius direction of the point
% --------
% 'img', a hypocotyl binary picture, is required for applying this scripts.

% define parameters
pace_min=0.1;
pace_max=0.7;
times_try_max=10;
radius_tolerance=1/100;
```

```
% scripts starts
pace=(pace_min+pace_max)/2;
i=1;
terminatebox=centralline_premeasurement(img);
% find termination box (locate around the cotyledon)
p(1)=centralline_initialize(img,ybottom);
% initialize the first point of hypocotyl
is_terminal=0;
while ~is_terminal
    times_try=0;
    i=i+1;
while ~is_centroid
       times_try=times_try+1;
if times_try>times_try_max;
          is_terminal=1;
% warnings, loggings and break.
break;
end
       p(i).c = NextPoint(p(i-1).c, p(i-1).v, p(i-1).r*pace);
% predict the next point position, (aligning?)the current point's
% tangent and moving pace is determined by last point's radius and
% pace factor.
       [p(i).v,p(i).rl,p(i).rr,p(i).vl,p(i).vr]=point_radius(img,
p(i));
       is_centroid = abs(p(i).rl-p(i).rr)/(p(i).rl+p(i).rr) <
radius_tolerance;
% ----  here, an error detection function is omitted ---- %
if is_centroid
% if current point fits the centroid good.
          pace = (pace_max+pace)/2;
% increase the pace factor for faster calculation.
          p(i).r = (p(i).rl+p(i).rr)/2;
else
% else, do the "centroid mending algorithm" mentioned in paper.
          A=p(i).rl;
          B=p(i).rr;
          Theta=ReformDirection(p(i).vr-p(i).vl);
% ^- the three quantitative values needed for "centroid mending algorithm"
          T=A/cos(Theta);
          X=T*(B-A)/(A+T);
% calculation of the mending offset along 'vr' or right vector
          ptemp=NextPoint(p(i).c,p(i).vr,X);
% an approximate mended point.
```

```
p(i-1).v=AbsDirection(GetDirection(p(i-1).c,ptemp),p(i-1).v);
% Changing the current point's tangent.
          pace=(pace_min+pace)/2;
% pace decreased for better precision.
end
end
% repeat until current point fits centroid good. usually takes
% 1-3 times for trying.
% -----Some error detection code is omitted ------ %
% ---Detected errors may also cause termination----%
    is_terminal = is_terminal || is_locate_in(p(i).c,terminatebox);
end



% Part 2:
% Pseudocode: terminus determination
% a centralline is a sequence of central point ( data structure point or
'p' )
% a centrallinelist is a sequence of centralline
% terminus determination can be applied after a correct centralline list
% is achieved.
% The sequence of binary images is assigned to img{n}

index_terminus(1)=terminal_point_initialize(centrallinelist{1});
% In current method, the point has most curvature is detected.

for i=1:numel(centrallinelist)-1
% generate target image around the index_terminus of current centralline
% generate a list of positions to scan. Scanlist is concentrated around
% the next centralline's terminus which is predicted from information
% provided by current centralline.

tar=generate_target(img(i),centrallinelist{i}(index_terminus(i)));
    scanlist=generate_scanlist(centrallinelist{i},index_terminus(i));

% caculating the Compare matrix, by the method
    C_rough=CompareMatrix(tar,img(i+1),scanlist);
    [~,min_index]=min(C_rough);
    min_scan=scanlist{min_index};

% refine the matching result:
    scanlist=generate_scanlist_refine(min_scan);
    C_fine=CompareMatrix(tar,img(i+1),scanlist);
```

```
    [~,min_index]=min(C_fine); % 2D minimum value
    min_scan=scanlist{min_index};
% ~90% time cost is saved by doing rough matching before refining.

% coordinate [min_x,min_y] may not fit with

index_terminus(i+1)=find_nearest_point(centrallinelist{i+1},min_scan)
;
end

% 'scan' is consist (consistent?) with a [x,y]. Cell 'scanlist' is consist
by a group of 'scan'.
function c=CompareMatrix(tar,field,scanlist)
[y,x]=size(tar);
for i=1:numel(scanlist)
    scan=scanlist{i};
    C=xor(tar,field(scan(2):scan(2)+y-1,scan(1):scan(1)+x-1));
    c(i)=sum(sum(C));
end
```